CONVERSION OF DMA DATA TO VISCOELASTIC MASTER CURVE AND PRONY SERIES FITTING

by

Batuhan Şahin

B.S., Civil Engineering, Istanbul Technical University, 2021

Submitted to the Institute for Graduate Studies in
Science and Engineering in partial fulfillment of
the requirements for the degree of
Master of Science

Graduate Program in Computational Science And Engineering
Boğaziçi University

2024

ACKNOWLEDGEMENTS

First and foremost, I would like to express my deepest gratitude to my supervisor, Prof. Şebnem Özüpek, for her invaluable guidance, support, and encouragement throughout this journey. Her expertise and patience have been a cornerstone in the successful completion of this thesis.

I am also profoundly grateful to the professors from whom I have had the privilege to take lectures during my academic journey. Their knowledge and dedication have not only enriched my understanding but have also inspired me to strive for excellence.

To my family and relatives, your unwavering love and support have been my anchor. Your belief in me has given me the strength to overcome challenges and stay focused on my goals.

Finally, I extend my heartfelt thanks to the people who are close to me, whose encouragement, understanding, and kindness have been a constant source of motivation. Your presence in my life has made this journey truly meaningful.

This thesis stands as a testament to the collective support and inspiration I have received, and I am forever grateful to each and every one of you.

ABSTRACT

CONVERSION OF DMA DATA TO VISCOELASTIC MASTER CURVE AND PRONY SERIES FITTING

This thesis details the process of converting Dynamic Mechanical Analysis (DMA) data of a viscoelastic material at different temperatures into a master curve. The methodology involves shifting DMA data based on the Williams-Landel-Ferry (WLF) universal constants and iteratively adjusting the shift to construct a continuous master curve. A Prony series is then fitted to the master curve, providing insights into the relaxation modulus at various temperatures. For the iteration a numerical method has developed using MATLAB. This process involves a comparison between the numerical iteration and the manual shifting using excel which is a criterion for the numerical iteration. Fitting Prony series is executed using MATLAB algorithms, for this instance Least Squares Algorithm is used. The developed numerical method is verified by comparing the results to those predicted from a Finite Element Analysis of a brain tissue subjected to compression loading.

ÖZET

DMA VERİLERİNİN VİSKOELASTİK ANA EĞRİYE DÖNÜŞTÜRÜLMESİ VE PRONY SERİSİ BULUNMASI

Bu tez, farklı sıcaklıklardaki viskoelastik bir malzemenin Dinamik Mekanik Analiz (DMA) verilerinin bir ana eğriye dönüştürülme sürecini detaylandırmaktadır. Metodoloji, Williams-Landel-Ferry (WLF) evrensel sabitlerine dayalı olarak DMA verilerinin kaydırılmasını ve sürekli bir ana eğri oluşturmak için tekrarlı kaydırmanın ayarlanmasını içerir. Daha sonra ana eğriye bir Prony serisi uydurarak çeşitli sıcaklıklardaki gevşeme modülüne ilişkin bilgiler sağlanır. Yineleme işlemi için MATLAB kullanılarak sayısal bir yöntem geliştirildi. Bu süreç, sayısal yineleme için bir kriter olan excel kullanılarak sayısal yineleme ile manuel kaydırma arasında bir karşılaştırmayı içerir. Prony serisinin uydurulması MATLAB algoritmaları kullanılarak yürütülür, bu örnek için En Küçük Kareler Algoritması kullanılır. Geliştirilen sayısal yöntem, sonuçların, basınç yüklemesine maruz kalan bir beyin dokusunun Sonlu Elemanlar Analizinden tahmin edilenlerle karşılaştırılmasıyla doğrulanır.

TABLE OF CONTENTS

LIST OF FIGURES

LIST OF TABLES

LIST OF SYMBOLS

a_t	Shift Factor
E_0	Instantaneous Modulus
E_∞	Equilibrium Modulus
E	Elastic Modulus
g	Spring Constant
T	Temperature
T_0	Reference Temperature
t	Time
η	Viscosity
ϵ	Strain
ϵ'	Strain Rate
ω	Frequency
ω_r	Reduced Frequency
τ	Relaxation Time
σ	Relaxation Modulus
$\sigma(t)$	Relaxation Modulus as a Function of Time
σ^*	Complex Modulus
σ'	Storage Modulus
σ''	Loss Modulus

LIST OF ACRONYMS/ABBREVIATIONS

2D	Two Dimensional
3D	Three Dimensional
DMA	Dynamic Mechanical Analysis
WLF	Williams–Landel–Ferry
Hz	Hertz

1. INTRODUCTION

Viscoelastic materials encompass a wide range of substances found in engineering, for instance biomedical naturally occuring materials such as biological tissues, tendons or ligaments and synthetic materials as rubber, plastics, polymers and memory foam materials. These materials are observed in everyday applications, such as energy absorbing elements as structural elastomers or biological structures as wood or tissue and cartilage. They exhibit time-dependent deformation under applied load. The fundamental understanding and accurate representation of viscoelastic behavior are paramount for predicting material response in diverse environments. Viscoelastic materials demonstrate a combination of viscous flow and elastic deformation when subjected to mechanical forces. This behavior arises from the internal friction and molecular rearrangement within the material structure. Unlike purely viscous materials, which exhibit continuous deformation under stress, viscoelastic materials also retain some degree of elastic behavior, allowing them to partially recover their original shape once the stress is removed. This time-dependent response makes viscoelastic materials highly versatile for various applications, ranging from damping materials to biological tissues.

In this Chapter fundamental features of viscoelasticity are described. Main goal of the study and the related literature review are presented. Finally particular objectives of the study and the outline of the thesis are given.

Uniaxial stress-strain response of an elastic and viscoelastic material can be seen in Figure 1.1. The difference occurs because of the energy loss which is due to viscous behavior. There are different types of tests to characterize the behavior of a viscoelastic material. These test measure the response either in time domain or frequency domain. Time domain tests include creep and stress-relaxation as shown in Figure 1.2.

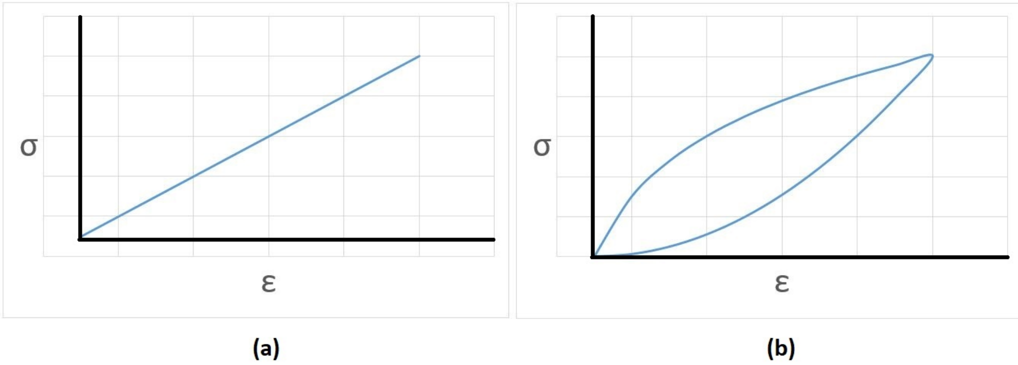

Figure 1.1. (a) Elastic and (b) Viscoelastic Loading-Unloading.

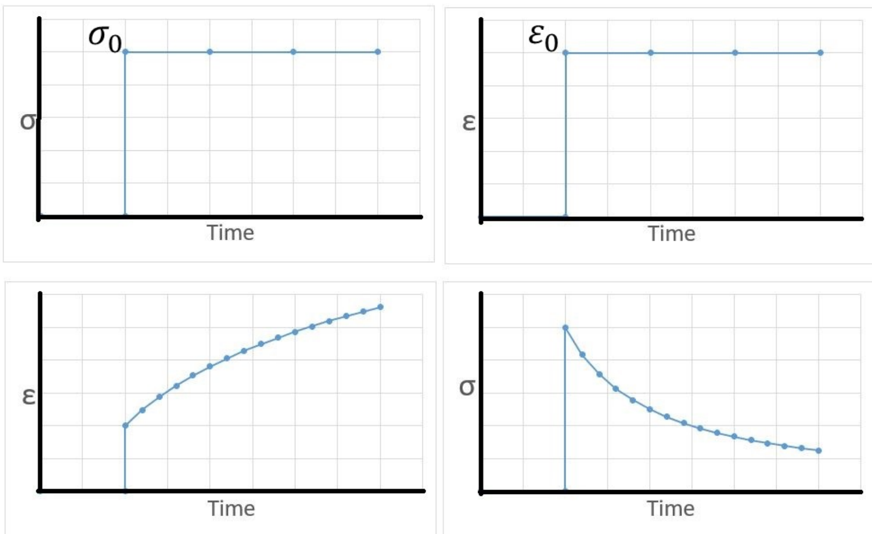

Figure 1.2. Creep (left) and Stress Relaxation (right)

In creep test, a step load is applied and the resulting time-dependent displacement is measured. Dividing the displacement by the undeformed length $\epsilon(t)$ is obtained. Dividing the applied load by the undeformed cross sectional area, σ_0 is obtained. Then creep compliance J(t) is defined as the ratio of the time dependent strain $\epsilon(t)$ to the corresponding stress σ_0 as:

$$J(t) = \frac{\epsilon(t)}{\sigma_0}. \tag{1.1}$$

In relaxation test, a step displacement is applied and the resulting time-dependent force is measured. Dividing the force by the undeformed cross sectional area, $\sigma(t)$ is obtained. Dividing the applied displacement by the undeformed length, ϵ_0 is obtained. Then relaxation modulus E(t) defined as the ratio of the time dependent stress $\sigma(t)$ to the corresponding strain ϵ_0 as:

$$E(t) = \frac{\sigma(t)}{\epsilon_0}. \tag{1.2}$$

To determine frequency domain response, Dynamic Mechanical Analysis (DMA) is used. In DMA test either the strain or the stress is applied sinusoidally and the stress or strain is monitored, as shown in Figure 1.3. If we were to observe an elastic material, stress and strain will be in phase. If we were to observe a viscous material, strain would be lagging behind stress at 90°phase angle. Figure 1.3 represents a viscoelastic material which has a phase angle between 0°and 90°.

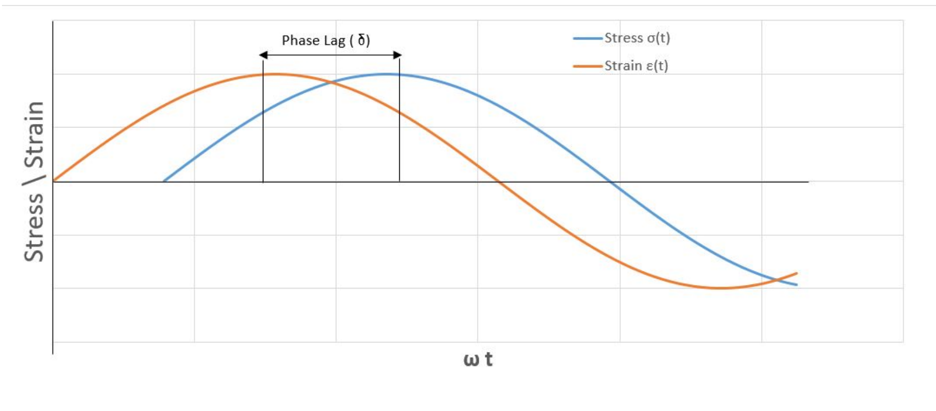

Figure 1.3. DMA test with time lag between stress and strain

Figure 1.3 represents the stress $\sigma(t)$ and strain $\epsilon(t)$ fuctions corresponds to,

$$\epsilon(t) = \epsilon_0 * sin(t\omega), \tag{1.3}$$

$$\sigma(t) = \sigma_0 * sin(t\omega + \delta). \tag{1.4}$$

Sinusoidal variation of stress and strain in the frequency domain gives complex modulus. From Equation 1.4:

$$\sigma(t) = [\sigma_0 * cos(\delta)] * sin(t\omega) + [\sigma_0 * sin(\delta)] * cos(t\omega) \tag{1.5}$$

where $\sigma_0 cos(\delta)$ is in phase with strain and $\sigma_0 sin(\delta)$ is 90°out of phase with the strain and δ is the phase lag. Equation 1.5 can be expressed in terms of storage modulus *E'* and loss modulus *E"* as

$$\sigma(t) = (E'\epsilon_0) * sin(t\omega) + (E''\epsilon_0) * cos(t\omega) \tag{1.6}$$

where,

$$E' = \frac{\sigma_0}{\epsilon_0} cos(\delta)\ ,\ E'' = \frac{\sigma_0}{\epsilon_0} sin(\delta) \text{ and } \frac{E''}{E'} = tan(\delta).$$

In the frequency domain, the linear viscoelastic behavior is described by the complex modulus *E**, described as:

$$E^*(\omega) = \frac{\tilde{\sigma}(\omega)}{\tilde{\epsilon}(\omega)}, \tag{1.7}$$

which is defined as the ratio of the complex stress $\tilde{\sigma}$ to the complex strain $\tilde{\epsilon}$ in terms of angular frequency ω and also described as:

$$E^*(\omega) = E'(\omega) + iE''(\omega), \tag{1.8}$$

where *E'* and *E"* are the real and imaginary parts, respectively.

Time domain tests have limitations such as inaccurate measurements for short time response and long testing times for equilibrium response. DMA, on the other hand, is simpler to perform and requires less testing time.

Temperature has a significant effect on the viscoelastic response. Mathematically this effect is represented using time- temperature or frequency - temperature superposition to generate a single response, called master curve, in terms of reduced time or reduced frequency.

Stress analysis of structures with viscoelastic materials may need to be performed in time or frequency domains. Therefore, it is important to have robust techniques that allows the interconversion of material properties between the two domains.

This thesis studies computational aspects of the mathematical representation of viscoelastic behaviour. In particular, the conversion of DMA data acquired at various temperatures into a comprehensive master curve is investigated.

In the following literature concerned with the interconversion between time and frequency domain representations of viscoelasticity is reviewed. The study [3] studies interconversion between the domains. Throughout the study integral transforms in between compliance modulus and relaxation modulus as well as complex compliance modulus and complex modulus are compared with general approximation equations. The approximations in this study is based on the inequalities and bounds of the response functions. Strain is considered as response when the stress is prescribed and stress is considered as response when the strain is prescribed. Inequalities are presented for a three parameter mechanical model. [6] mentions Prony series fitting, using a defined log-sigmoidal function to smooth source data and a linear program technique to obtain Prony series coefficients with constraints. [4] employs numerical techniques of the transitory viscoelastic equations which takes root from Prony representation. Relying on experimental data, for converting between linear viscoelastic material properties using a Prony series. In [5] a novel, highly straightforward method which includes approximate linear viscoelastic equations for interconversion, approximate Laplace transformations as well as reversal for these equations is proposed. These methods were validated through sample demonstrations.

So far we have mentioned the studies fundamental for our study. And now we can mention the studies parallel to ours. In the study [7] it is examined the impact of loading frequency and temperature on the dynamic mechanical behavior of asphalt mixture containing basalt fiber. Furthermore, utilizing the time-temperature superposition principle, master curves of complex modulus were developed to represent the dynamic mechanical response over an expanded range of reduced frequencies at any given temperature. Another study [9] uses creep experiments on a viscoelastic material asphalt shingles. The creep experiments are done in different temperatures. Study continues with constructing a master curve and fitting WLF parameters and concludes with fitting the Prony series to the constructed master curve.

The objectives of the thesis are following:

(i) Conversion of DMA data acquired at various temperatures into a comprehensive master curve. The process involves two primary stages:

(ii) First, the utilization of the Williams-Landel-Ferry (WLF) universal constants for shifting DMA data,

(iii) Second, the construction of a continuous master curve through iterative adjustments.

(iv) A key aspect of this thesis is the exploration of different custom functions in conjunction with the least squares algorithm for fitting Prony series constants as one of the initial concern for this study will be the numerical analysis.

(v) The issue with the viscoelastic material is the definition of mechanical properties, the tests can be applied in time domain such as relaxation test or in frequency domain such as Dynamic Mechanical Analysis, we also expect for our analysis to have convergence to the tests in any domain. This approach seeks not only the optimal fit but also a deeper understanding of the viscoelastic behavior by constructing the master curve of the material across different temperature regimes.

The integration of these methods aims to enhance the accuracy and reliability of the resulting master curve, providing valuable insights into the material's dynamic response under varying conditions. The verification will be done via using ABAQUS by creating the optimal geometry and corresponding analysis using the data from the studies [1] and [2]. Also the data obtained from[13] which also includes a manual analysis for constructing the master curve.

In Chapter 2 different mechanical models and constitutive equations representing viscoelastic behavior in both time and frequency domain are described. The representation of temperature effect is also presented. In Chapter 3 the methodology is explained. Methodology consists of searching for the optimal mathematical equations (which depends on the factors of Prony coefficients) for Prony series fit (Mathematical Representation of Viscoelastic Behavior) using least squares algorithm, followed by the temperature dependent shifting, and iteration for the construction of master curve. In Chapter 4 verification of the resulting material model on time and frequency domains is presented. In Chapter 5 Prony series calibration with an alternative data set and the use of the resulting model in cyclic analysis is presented. Conclusions and future work are discussed in Chapter 6.

2. BACKGROUND

2.1. Mechanical Models

Viscoelastic material response can be represented with mechanical models. Since viscoelastic material behaves both as elastic and viscous, the mechanical models contain a spring and a dashpot simulating the behavior of the material. Different combination of spring and dashpot, results in different constitutive equations.

Using the following stress, σ, and strain, ϵ, relations for the spring,

$$\sigma = E * \epsilon \tag{2.1}$$

and for the dashpot,

$$\sigma = \mu * \frac{d\epsilon}{dt} \tag{2.2}$$

and relating spring stiffness, E, and dashpot viscosity, μ through

$$\tau = \frac{\mu}{E}, \tag{2.3}$$

various mechanical model can be constructed.

Maxwell model illustrated in Figure 2.1 is constituted with a spring and a dashpot in series.

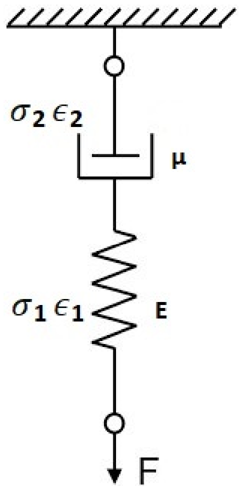

Figure 2.1. Maxwell Model

Using,

$$\sigma = \sigma_1 = \sigma_2 \tag{2.4}$$

$$\epsilon = \epsilon_1 + \epsilon_2 \tag{2.5}$$

we have the constitutive equation presented as:

$$\sigma + \tau * \frac{\partial \sigma}{\partial t} = E * \tau * \frac{\partial \epsilon}{\partial t}. \tag{2.6}$$

Kelvin-Voigt model illustrated in Figure 2.2 is constituted with a spring and a dashpot in parallel.

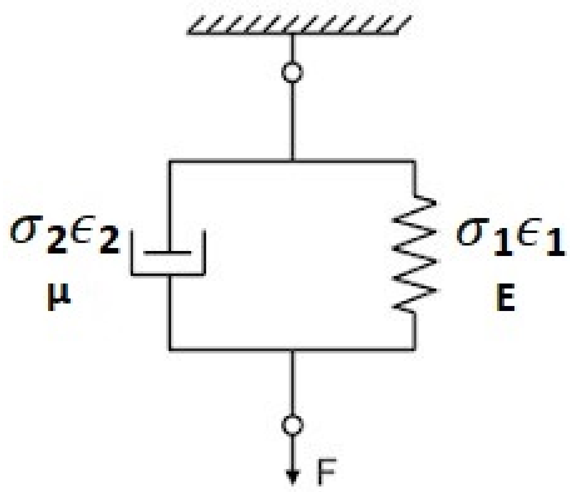

Figure 2.2. Kelvin-Voigt Model

Using,

$$\sigma = \sigma_1 + \sigma_2, \tag{2.7}$$

$$\epsilon = \epsilon_1 = \epsilon_2, \tag{2.8}$$

we have the constitutive equation presented as:

$$\sigma = E * \epsilon + E * \tau * \frac{\partial \epsilon}{\partial t}. \tag{2.9}$$

Standard linear solid model is illustrated in Figure 2.3 where a spring and a Maxwell model are constituted in parallel. Constitutive equation for this model is as follows,

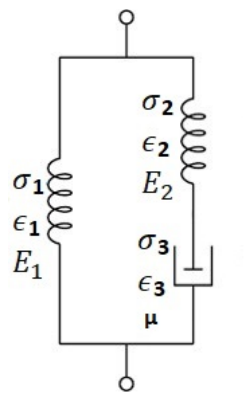

Figure 2.3. Standard Linear Solid Model

Using,

$$\sigma = \sigma_1 + \sigma_2, \tag{2.10}$$

$$\epsilon = \epsilon_1 = \epsilon_2 + \epsilon_3, \tag{2.11}$$

$$\sigma_2 = \sigma_3, \tag{2.12}$$

we have the constitutive equation presented as:

$$\sigma + \tau * \frac{\partial \epsilon}{\partial t} = E_1 * \epsilon + (E_1 + E_2) * \tau * \frac{\partial \epsilon}{\partial t}. \tag{2.13}$$

As the mechanical models shown in Figures 2.1, 2.2 and 2.3 are simple representations of viscoelasticity and do not completely describe the material, a more complex model which consists of multiple Maxwell models connected in series or in parallel named as generalized Maxwell model is constructed. This model enables a realistic viscoelastic behaviour.

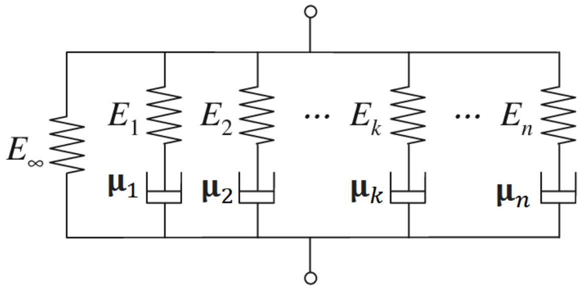

Figure 2.4. Generalized Maxwell model.

Because the Generalized Maxwell model is a more complex mechanical model, the governing differantial equation comes out as:

$$a_0\sigma + a_1\frac{d\sigma}{dt} + a_2\frac{d^2\sigma}{d^2t} + ... = b_0\epsilon + b_1\frac{d\epsilon}{dt} + b_2\frac{d^2\epsilon}{d^2t} + ... \tag{2.14}$$

2.2. Integral Models

Integral constitutive equations are alternative to mechanical model which are in differential form. In particular, a convolution integral is used to represent the linear viscoelastic behaviour as:

$$\sigma(t) = E_\infty * \epsilon(t) + \int_0^t R(t-t') * \dot{\epsilon}(t')dt. \tag{2.15}$$

In Equation 2.15, $\sigma(t)$, that is the stress at time t. E_∞ is the equilibrium modulus, $\epsilon(t)$ is the strain at time t and $R(t)$ is the relaxation function.
The Prony series is commonly used for a mathematical representation of $E(t)$. It decomposes the relaxation spectrum into a sum of exponential terms, each characterized by a relaxation time τ_i and the corresponding coefficient E_i, and is expressed as:

$$E(t) = E_\infty + \sum_{i=1}^{N} E_i * e^{\frac{-(t)}{\tau_i}}. \tag{2.16}$$

Equation 2.16 illustrates relaxation modulus *E(t)* at time *t*. The Prony series model can also be interpreted in terms of a spring-dashpot network, where each term in the series corresponds to a spring-dashpot element. The exponential term represents the behavior of a dashpot, which dissipates energy over time, while the coefficient represents the behavior of a spring, which stores and releases energy. By summing the contributions from multiple spring-dashpot elements, the Prony series model captures the complex viscoelastic behavior of the material and is equivalent to generalized Maxwell model.

By fitting the Prony series parameters to experimental data, the relaxation behavior of viscoelastic materials can be accurately characterized, allowing for the prediction of material response under different loading conditions. The Prony series model provides valuable insights into the material's dynamic mechanical properties and is widely used in computational design and analysis tools.

2.3. Frequency Domain Representation

The Prony series can be expressed in the frequency domain by considering Fourier transformation of the integral equation. From Equation 2.15:

$$\tilde{\sigma}(\omega) = E_\infty \tilde{\epsilon}(\omega) + \tilde{R}(\omega) i\omega \tilde{\epsilon}(\omega) \tag{2.17}$$

or

$$\tilde{\sigma}(\omega) = E^*(\omega)\tilde{\epsilon}(\omega) \tag{2.18}$$

where

$$E^*(\omega) = E_\infty + i\omega \tilde{R}(\omega). \tag{2.19}$$

From the time domain equation, Equation 2.16, we obtain frequency domain equation,

$$\tilde{R}(\omega) = \sum_{1}^{N} \frac{E_k}{\frac{1}{\tau_k} + i\omega} \tag{2.20}$$

so that

$$E^*(\omega) = E_\infty + i\omega \sum_{1}^{N} \frac{E_k}{\frac{1}{\tau_k} + i\omega}. \tag{2.21}$$

Decomposing Equation 2.21 into a real part $E'(\omega)$ (storage modulus) and an imaginary part $E''(\omega)$ (loss modulus), and recalling the complex modulus, E^*, as:

$$E^*(\omega) = E'(\omega) + i * E''(\omega) \tag{2.22}$$

we obtain

$$E' = E_\infty + \sum_{1}^{N} \frac{E_k * \omega^2 * \tau_k^2}{1 + \omega^2 * \tau_k^2}, \tag{2.23}$$

$$E'' = \sum_{1}^{N} \frac{E_k * \omega * \tau_k}{1 + \omega^2 * \tau_k^2}. \tag{2.24}$$

2.4. Rerpresentation Of The Temperature Effect

Temperature effect is commonly taken into acount through the time-temperature superposition, that is viscoelastic behaviour at one temperature is related to another by a change in the time scale only. First, a reference temperature,T_0 is selected, then relaxation curves at other temperatures are horizontally shifted on a logarithmic time scale to obtain a single curve called the master curve. The amount of shift is called the shift factor, a_T, and is a function of temperature, T. The horizontal axis time ,t , is replaced by the reduced time in, t_r ,as

$$t_r = \frac{t}{a_T}. \tag{2.25}$$

The Williams-Landel-Ferry (WLF) model is commonly used to represent the shift factor dependence on temperature as:

$$\log(a_T) = \frac{-C_1(T - T_0)}{C_2 + (T - T_0)} \tag{2.26}$$

where C_1 and C_2 are parametes to be fitted according to the material data. Also acknowledged universal constants for these parameters are respectively 17,44 and 51,6.

The same shift factor is used to apply frequency-temperature superposition.

The WLF model provides a simple means to represent the change in viscoelastic behavior with temperature, allowing for the extrapolation of material properties over a range of temperatures. Understanding the temperature dependence of viscoelastic materials is essential for designing materials that perform reliably under different environmental conditions.

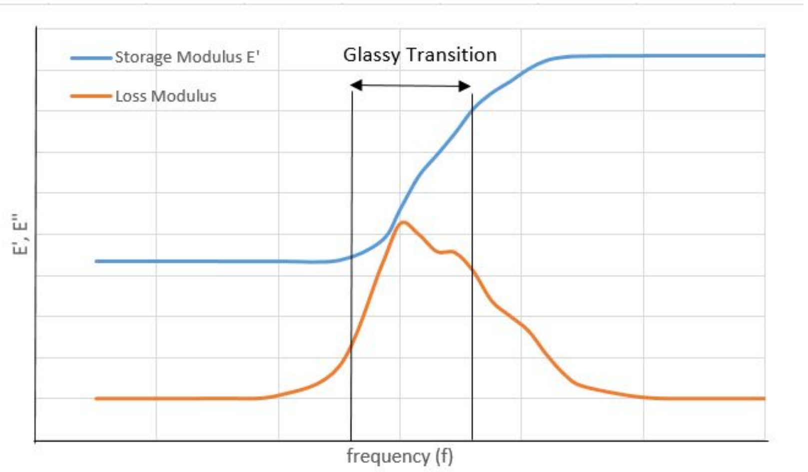

Figure 2.5. Different Regions for Different Frequencies (Different Temperatures) [11]

Figure 2.5 shows a typical behaviour of a viscoelastic material storage modulus and loss modulus over a wide range of frequency which was acquired through time-temperature superposition fundamentals in this thesis. In the study we aim to construct such a master curve via time-temperature superposition.

3. METHODS

3.1. Preliminary Prony Series Fitting

As mentioned in Chapter 2, relaxation curve is often is expressed in frequency or time domain. In this study the Prony series will be fit to data given in frequency domain. The initial step aimed to find a suitable Prony fit procedure, therefore various types of Prony series fits were attempted using a least squares algorithm to identify the optimal function for describing the viscoelastic behavior. The criteria for optimization is to accurately obtain a Prony series fit to storage and loss modulus, which accurately represents relaxation modulus as well.
Prony parameters to be determined are the coefficients E_i and relaxation times τ_i. These are seen in Equation 3.1 and Equation 3.2 for the storage and loss moduli and Equation 3.3 for the relaxation modulus. The dependence and factor of these parameters affects the convergence of the series. In the figure 3.1 different custom equations has been fit to the data to see the difference of the error so that we can find a optimal fit for the prony series. First custom equations consists storage modulus,E' , which is the real part of the complex modulus is given as:

$$E' = E_e + \sum_{1}^{N} \frac{E_i * \omega^2 * \tau_i^2}{1 + \omega^2 * \tau_i^2} \tag{3.1}$$

and loss modulus, E", which is the imaginary part of the complex modulus

$$E'' = \sum_{1}^{N} \frac{E_i * \omega * \tau_i}{1 + \omega^2 * \tau_i^2} \tag{3.2}$$

also relaxation modulus, E, which is the time domain representation of the equations

$$E = E_e + \sum_{1}^{N} E_i * e^{\frac{(-t)}{\tau_i}}. \tag{3.3}$$

We fit both Equation 3.1 and Equation 3.2 simultaneously or one of these equations to the storage and loss modulus data obtained from literature. For the preliminary Prony series fit DMA data from the papers Tapia-Romero [1] and Weiqi Li [2] are used. Data obtained from these papers are for different materials and have both time domain and frequency domain test results which are important for this study. The fit is done in Matlab [10] using the least squares method. In Equation 3.1 or Equation 3.2 there are $2N$ parameters to be determined. In the second custom, only one factor of relaxation time was considered as unknown, the other relaxation times were asumed to change decade apart. The resulting equation becomes

$$E' = E_e + \sum_{1}^{N} \frac{E_i * \omega^2 * (\tau * (10^(N-5))^2}{1 + \omega^2 * (\tau * (10^(N-5))^2} \tag{3.4}$$

and is the blue labeled curve in Figure 3.1 . The following fit (third custom equation) considered N number of E_i and τ_i where τ_i were taken a decade apart, as:

$$E' = E_e + \sum_{1}^{N} \frac{E_i * \omega^2 * (\tau_i * (10^(N-5))^2}{1 + \omega^2 * (\tau_i * (10^(N-5))^2} \tag{3.5}$$

and the resulting fit is shown in Figure 3.1 with green fit. Finally, fitting of N number of E_i and τ_i parameters considered as seen Equation 3.1 with the resulting fit shown in red in Figure 3.1.

According to Figure 3.1 the best fit is for Equation 3.4 which is the blue labeled fit. The Prony fit was compared to relaxation curve data in Figure 3.1.

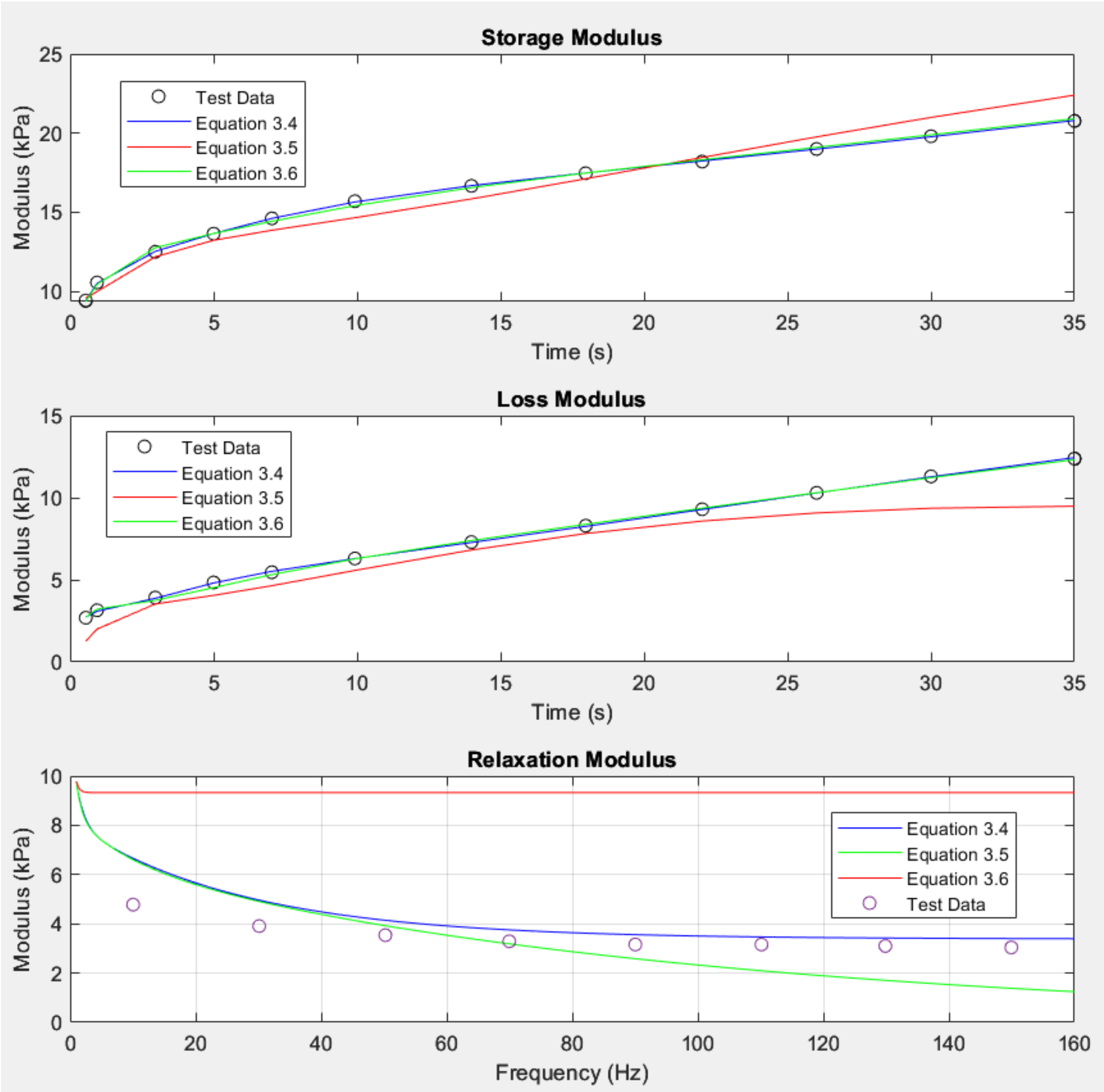

Figure 3.1. Prony fits for different functions.

3.2. Master Curve Construction

To construct the master curve we will be using data at various temperature [12]. The data shown in Figure 3.2 is obtained from a DMA at different temperatures in a frequency range of 0.1 Hz to 100 Hz. As can be seen in Equation 2.26 shift factors are calculated for modulus plotted in the logarithmic frequency. By use of this data it will be possible to create a master curve by shifting the data and determining the shift factors.

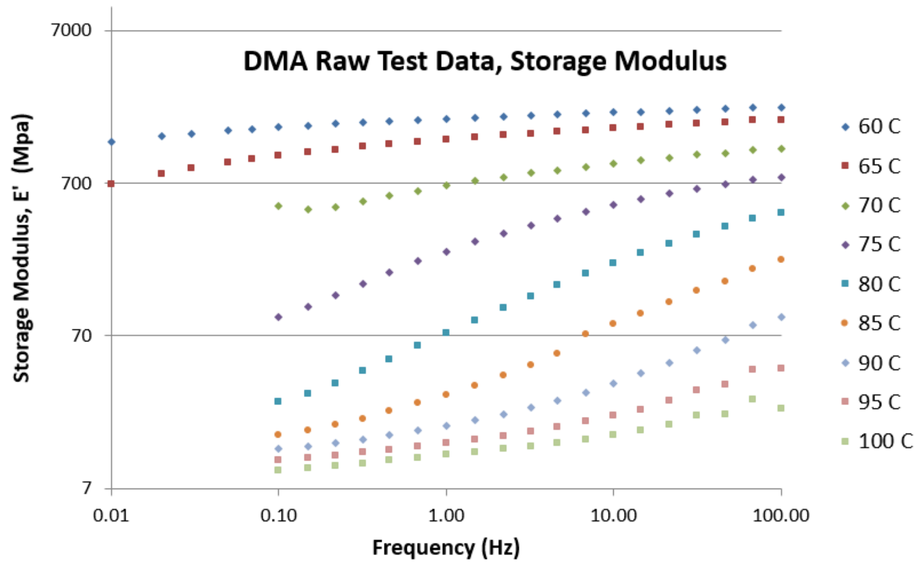

Figure 3.2. DMA Data For Each Temperature [12]

Shifting of raw data is done with respect to a reference temperature which was selected as 75°. The initial estimate for shift factor was obtained from WLF equation using the universal constants given as $C_1 = 17,44$ and $C_2 = 51,6$ [14]. After this shifting, initial master curve is constructed. As seen from Figure 3.3 discontiunity in the master curve is observed. To measure the discontiunity a preliminary error is defined. The error norm is defined as the area of the overlapping region and was used as a criterion for assessing the need for additional shifts. Figure 3.3 illustrates the initial shifting results.The continuity corresponds to the overlapping region of each consecutive temperature curve.

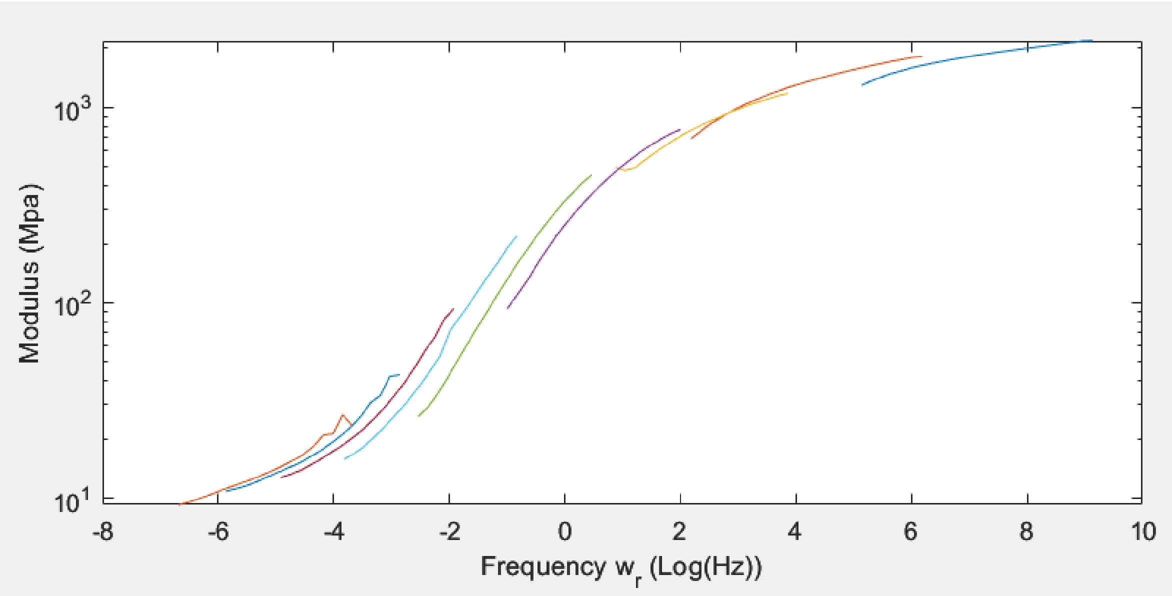

Figure 3.3. DMA Data For Each Temperature

3.3. Iterative Shifting

In this section an iterative process is applied to the shifted data to acquire the continuity of the master curve. The algorithm behind this process is illustrated in Figure 3.4 with a flowchart. This flowchart consists of two loops. First loop consists of unit shifting, overlapping index calculation and error calculation. This loop continues for maximum of 150 steps or less depending on the error. And according to the error calculation flow continues with the second loop. Second loop becomes effective for unsatisfactory error output.

3.3.1. First Loop

Iteration step starts with unit shifting in terms of reduced frequency as $\log(\omega_r) = 0.1$. Each modulus curve is shifted with respect to the neighboring curve.

In order to calculate the error we define hundred indices between the beginning and ending points of overlapping region as seen in Figure 3.5. Each index corresponds to a modulus and a frequency value which is stored in the arrays SM and $LogF$ respectively. As the overlapping region is between two temperature curves, we used subscripts (upper and lower) for the arrays to indicate the different temperature curves. Overlapping region for the upper temperature cuve is defined as the begining of the $LogF_{Upper}$ until an index J which corresponds to the ending of the $LogF_{Lower}$. Similarly overlapping region for the lower temperature cuve is defined as the ending of the $LogF_{Lower}$ from an index K which corresponds to the beginning of the $LogF_{Upper}$. With every step new indexes are calculated and according to new indexes new error is calculated.

The error is calculated as the ratio of the absolute trapezoidal area in between the temperature curves to the trapezoidal area under the lower temperature curve. The change in the error is illustrated in Figures 3.5 and 3.6 before and after the iteration, respectively. Figure 3.5 illustrates the error (area), which is bounded by the overlapping region and calculated as:

$$[\frac{|SM_{Upper}[K] - SM_{Lower}[1]|}{SM_{Lower}[1]} + \frac{|SM_{Upper}[100] - SM_{Lower}[J]|}{SM_{Lower}[J]}]. \tag{3.6}$$

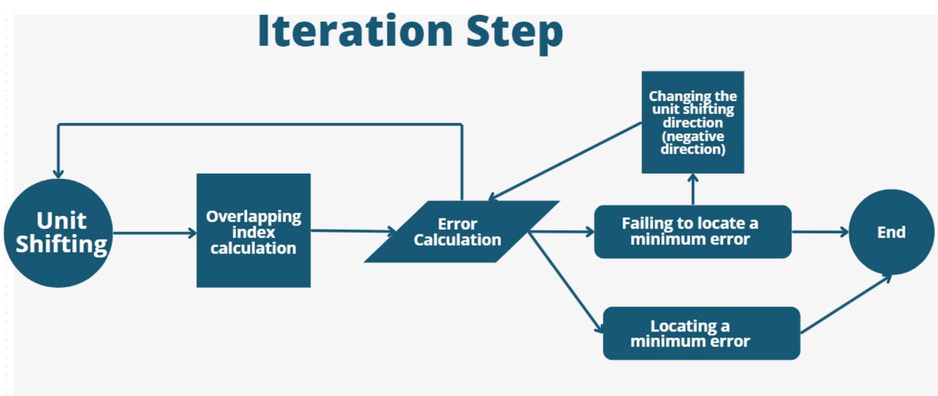

Figure 3.4. Flow chart of the iteration

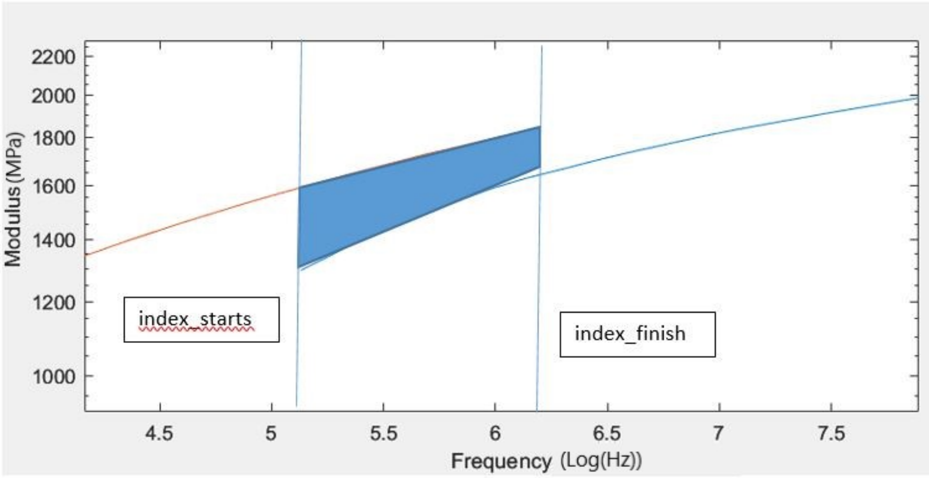

Figure 3.5. Initial overlapping region, shifted according to universal constants of WLF equation.

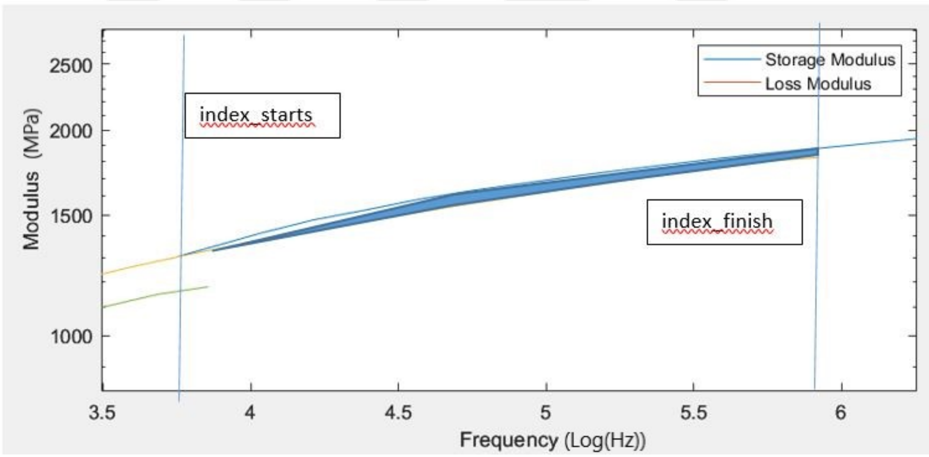

Figure 3.6. Final overlapping region, shifted according to the algorithm mentioned above. Iteration continues until desired error is satisfied.

3.3.2. Second Loop

Second loop consists of reversal of unit shifting direction. If a minimum error is observed in the error calculation, the index corresponding to the minimum error is recorded to be used in determining shift factor. Examples are illustrated in Figures 3.7 and 3.8. According to the output of the initial loop, iteration cleaves. Hence a second loop is defined.

If during 150 steps a minimum error is not reached at the end of first loop, the error at step one becomes the minimum, therefore the corresponding index is assigned as the initial index and the direction for the unit shifting is reversed. After this alternation the flow follows the first loop. Examples where direction reversal is done are shown in Figure 3.9, Figure 3.10, Figure 3.11 and Figure 3.12.

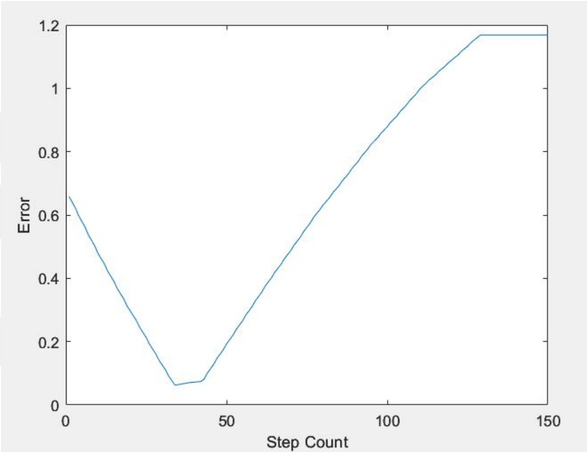

Figure 3.7. Error for steps between 75°C - 80°C curves(5th iteration step)

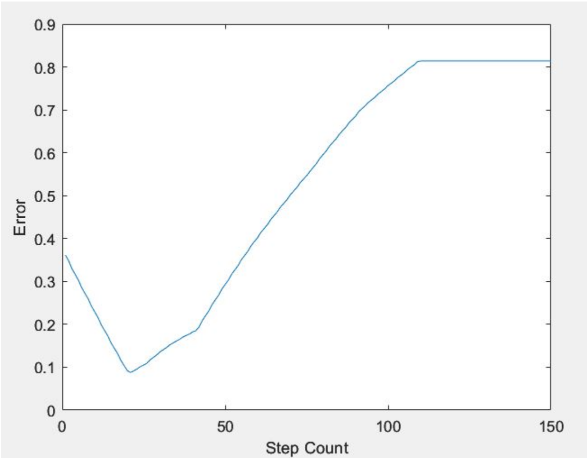

Figure 3.8. Error for steps between 70°C - 75°C curves(6th iteration step)

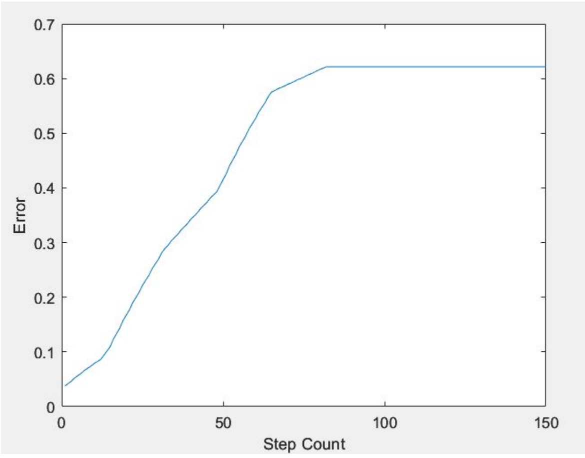

Figure 3.9. Error for positive steps between 60°C - 65°C curves (8th iteration step)

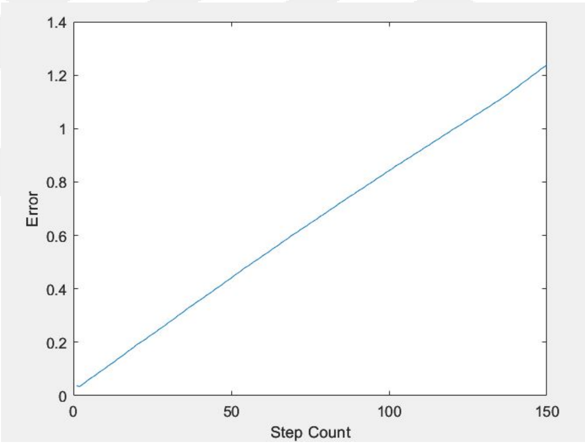

Figure 3.10. Error for negative steps between 60°C - 65°C curves (8th iteration step)

In Figure 3.10 plateau is observed almost at starting point, this indicates that in Figure 3.9 the minimum point is sligthy behind of the initial index.

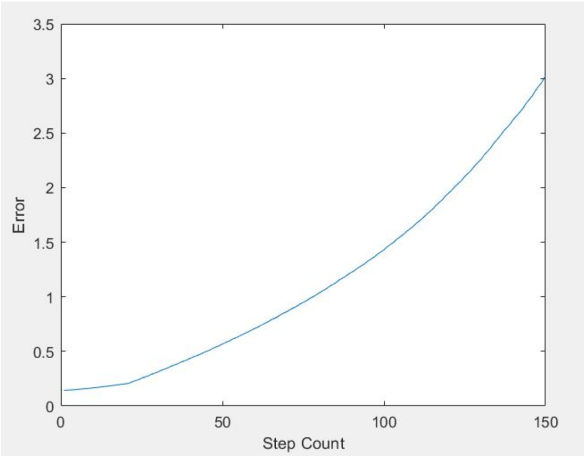

Figure 3.11. Error for positive steps between 85°C - 90°C curves (3rd iteration step)

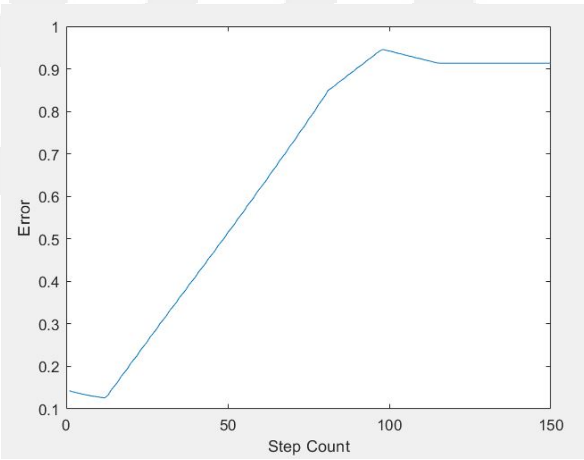

Figure 3.12. Error for negative steps between 85°C - 90°C curves (3rd iteration step)

Figure 3.11 and Figure 3.12 also belong to same iteration. When the unit shifting value is reversed, plateau is reached.

Table 3.1. Shifting Values with respect to the Preceeeding Temperature Curve.

	60°C	**65°C**	**70°C**	**75°C**	**80°C**	**85°C**	**90°C**	**95°C**	**100°C**
Shift Factors	-0.02	0.18	0.21	0.34	0.32	-0.12	0.25	1.5	0

Afterwards, the reference temperature was selected as 75°and the shift factors were adjusted accordingly. This process basically includes adding shifting values one after the other so that distance from the reference temperature curve is calculated.The resulting values are seen in Tables 3.2.

Table 3.2. Shifting Values with respect to the Reference Temperature Curve.

	60°C	**65°C**	**70°C**	**75°C**	**80°C**	**85°C**	**90°C**	**95°C**	**100°C**
Shift Factors	5.50	4.05	1.98	0	-1.21	-2.16	-3.04	-3.81	-4.64

The master storage and loss moduli are shown in Figure 3.13 which are constructed using the shift factors given in Table 3.2. The shifting was done for the storage modulus data and the resulting shift factors were used to construct the master loss modulus.

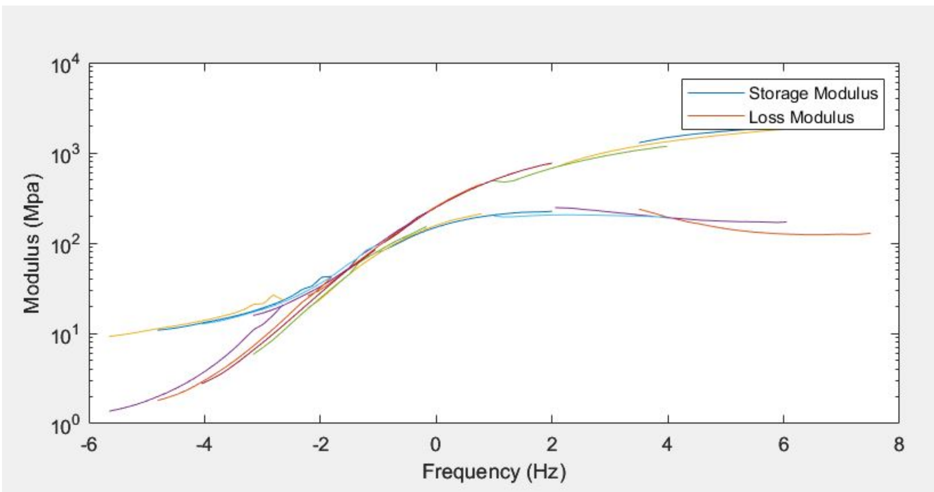

Figure 3.13. Finalised Shifted Temperature Curves (Storage and Loss Modulus)

3.4. Overlapping Data Reduction

The master curve shown in Figure 3.13 is to be used for the fitting of Prony series. In order to have a sensible fitting any overlapping data resulting from the iterative shifting process need to be eliminated, hence a method was introduced to cut redundant portions and ensure a continuous master curve. This involved identifying overlapping regions and trimming the data to eliminate redundancies, thereby enhancing the overall continuity of the master curve. This elimination is based on the index values corresponding to the beginning and ending of the overlapping and the construction of the master curve as an array where we chose only one set of data for the overlap. In Figure 3.13 we see the overlapping data and in Figure 3.14 we observe the clipped data.

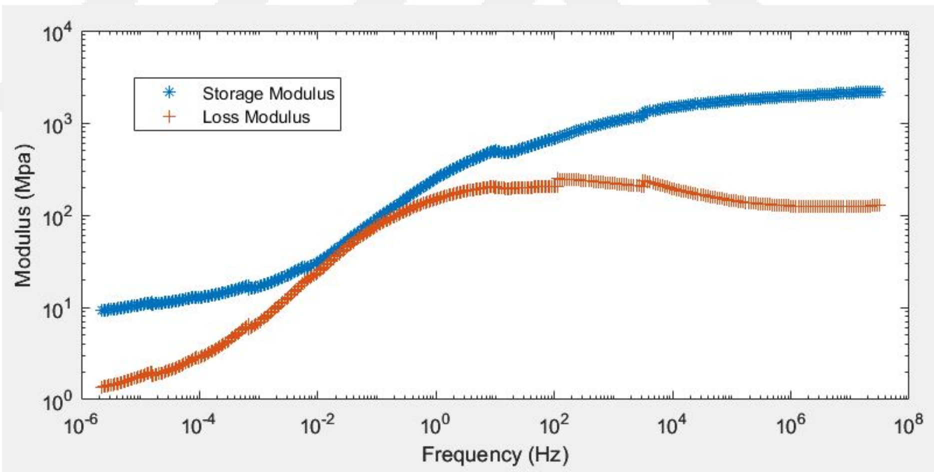

Figure 3.14. Clipped Temperature Curves (Storage and Loss Modulus)

3.5. WLF Parameters

Shift factors listed in Table 3.2 can be used to determine the shift factor for any temperature using interpolation. Alternatively WLF parameters given in Equation 2.26 can be determined by curve fitting to this data. Availability of WLF function is important since this form is widely used in computational analysis software. Figure

3.15 demonstrates the resulting fit for the WLF equation,

$$\log(\frac{t}{a_t}) = \frac{-C_1(T - T_0)}{C_2 + (T - T_0)}, \tag{3.7}$$

where least squares algorithm was used. WLF coefficients are given in Table 3.3.

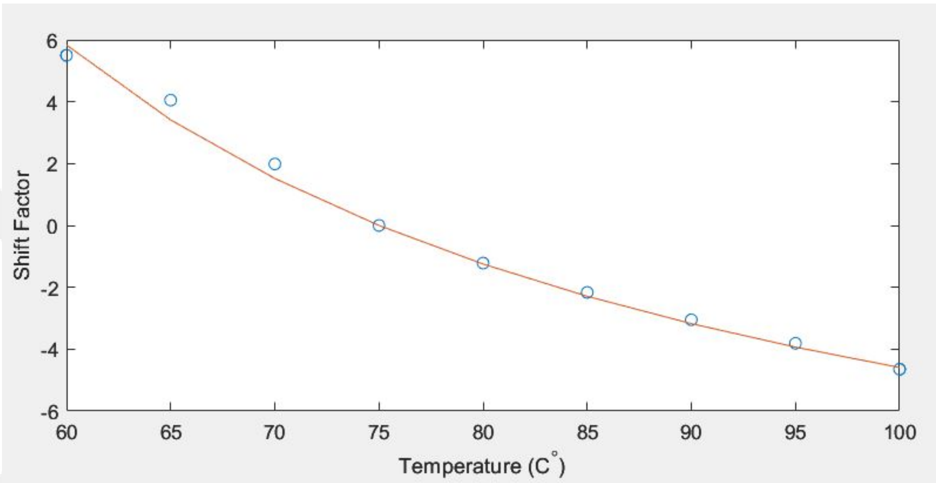

Figure 3.15. Shift factor for each temperature and WLF fit

Table 3.3. WLF Coefficients fit with Least Squares Algorithm.

	C_1	C_2
Universal Constants	17.44	51.6°C
WLF Fit from iteration	13.93	50.83°C
Reference temperature (T_0)	**75°C**	

3.6. Prony Series Fitting of Master Curve

Once a continuous master curve was obtained and redundant data was eliminated, Prony series was fitted to the resulting data. The Prony series model was chosen based on the results of the preliminary fitting attempts presented in Section 3.1, ensuring a

robust representation of the viscoelastic material's behavior. A result of preliminary analysis presented in Section 3.1, the Equation 3.4 was used. The parameters for this function were fitted using least squares algorithm. These parameters include N number of relaxation coefficients, E_i, and one relaxation time with other relaxation times decade apart (N number of spring parameters and one dashpot parameter were fitted, as one dashpot parameter is the coefficient for N number of exponentially growing relaxation times) also an equlibrium modulus. For this master curve fitting N was chosen as 14. At this point as DMA data exists for both storage modulus and loss modulus, the algorithm was adjusted to fit the series using only storage modulus data or using both moduli.
Case 1 consists of simultaneous fit for both storage and loss modulus data. Case 2 consists of only storage modulus fit. The results are shown in Figure 3.16 thru Figure 3.19.

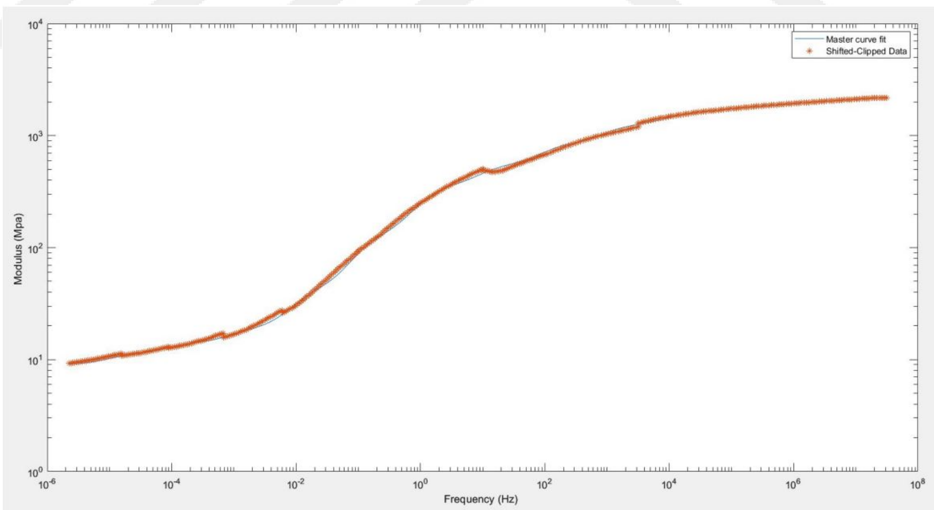

Figure 3.16. Storage Modulus data and Case 1 Prony Series Fit

Figure 3.16 and 3.17 compare test data to the storage and loss moduli, respectively, for Case 1.

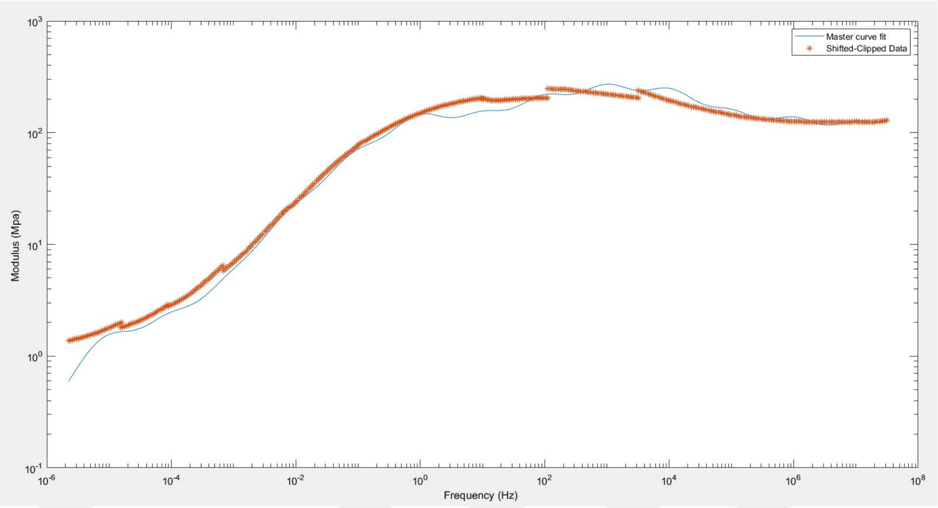

Figure 3.17. Loss Modulus data and Case 1 Prony series Fit

Figures 3.18 and 3.19 compare test data to the storage and loss moduli, respectively, for Case 2.

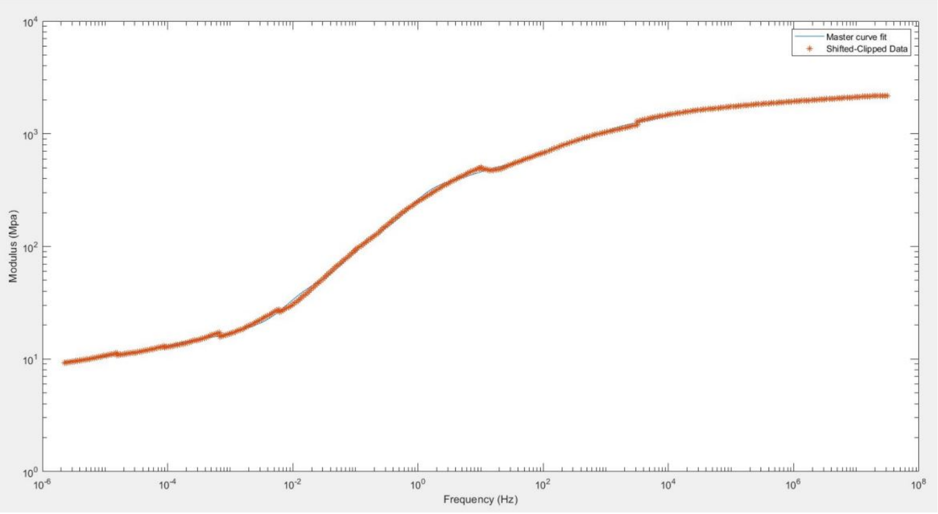

Figure 3.18. Storage Modulus data and Case 2 Prony Series Fit

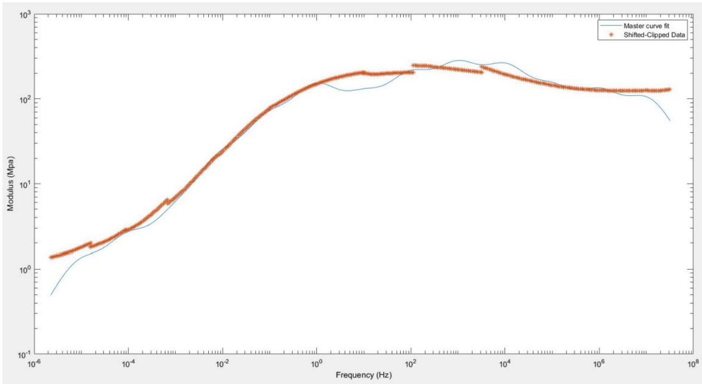

Figure 3.19. Loss Modulus data and Case 2 Prony series Fit

The Prony parameters are given in Tables 3.4 and 3.5 for Case 1 and Case 2.

Table 3.4. Prony Series Fits for Case 1.

	Coefficients, E_i (MPa)	**Relaxation times, τ_i (s)**
E_∞	9.0047	
1	252.4062	10^{-8}
2	161.7630	10^{-7}
3	192.4685	10^{-6}
4	201.1384	10^{-5}
5	369.7725	10^{-4}
6	400.5051	10^{-3}
7	309.2691	10^{-2}
8	195.2972	10^{-1}
9	230.3223	10^{0}
10	87.7006	10^{1}
11	23.3427	10^{2}
12	4.5957	10^{3}
13	2.8851	10^{4}
14	2.3968	10^{5}

Table 3.5. Prony Series Fits for Case 2.

	Coefficients, E_i (Mpa)	**Relaxation times, τ_i (s)**
E_∞	9.4967	
1	2.2537e-05	10^{-8}
2	169.5849	10^{-7}
3	191.1797	10^{-6}
4	184.4500	10^{-5}
5	399.1900	10^{-4}
6	419.5676	10^{-3}
7	309.9359	10^{-2}
8	140.1636	10^{-1}
9	255.0382	10^{0}
10	85.4947	10^{1}
11	27.9387	10^{2}
12	3.8960	10^{3}
13	3.5509	10^{4}
14	1.8632	10^{5}

For both cases, the storage modulus fit is adequate. The loss modulus has a better fit for Case 1.

3.7. Time Domain Prony Series

Using the Prony parameters determined in Section 3.6 time domain relaxation modulus was calculated using Equation 2.16. The resulting curves are shown in Figure 3.20. In addition with the shift factors determined in Table 3.2, relaxation modulus for various temperatures was calculated using,

$$E_T(t) = E_\infty + \sum_{i=1}^{N} E_i * e^{\frac{(-t)}{10^{(\log\tau_i + Shift)}}}. \tag{3.8}$$

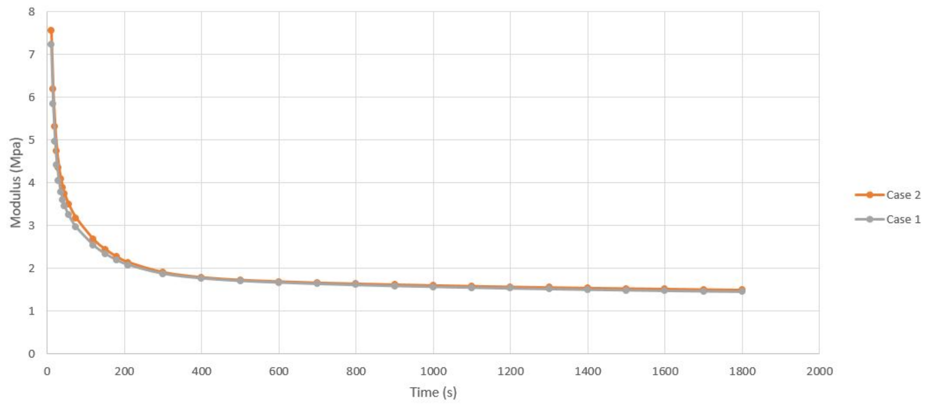

Figure 3.20. Time Domain Prony Series For Case 1 and 2

The resulting curve is shown in Figure 3.21.

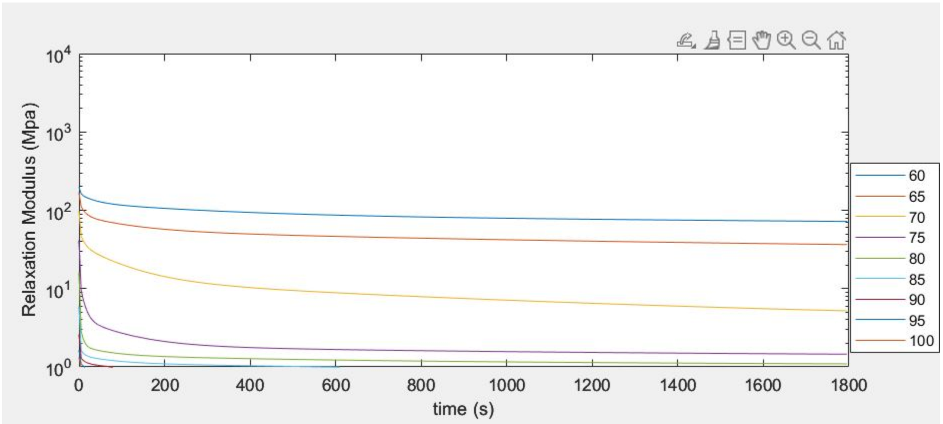

Figure 3.21. Relaxation modulus for each temperature

3.8. Conclusion

Conversion of frequency domain to time domain is done with Prony series coefficient. In case both time and frequency domain tests are available, a better fit with prony series is possible. Prony series for the mentioned case can be fitted with certain constraints such as instantaneous or long-term modulus which will illustrate a realistic fit and interconversion.

Another matter is the shift factors. As can be seen in Figure 3.21, not only the conversion is done but also using the shift factors breakdown of the relaxation modulus for different temperatures is done. If time domain data were avaliable for different temperatures, this can give an idea over the shift factors and eventually the master curve.

4. MATERIAL MODEL VERIFICATION VIA ABAQUS

The validation of the code developed in Matlab and presented in Chapter 3 was done using ABAQUS. A simple 2D model subjected to tension was analyzed for the study [12]. Model consist of 80 nodes as seen in Figure 4.1. CPS4R elements were used. Boundary conditions for this body are shown in Figure 4.2 and consist of symmetry condition on the left and no displacement on the bottom. Material is defined as linear viscoelastic using the Prony series given in Table 3.4. Instantaneous modulus is used for the elastic part and Prony series is used as the viscoelastic part. The temperature effect is defined using WLF coefficients. Using properties calculated in this study model 1 is constructed and using porperties given in [12] model 2 is constructed in ABAQUS. Same analysis is applied to both models. Loading was applied as a displacement to the top part of the body. In time domain a dynamic analysis and in frequency domain a steady-state dynamic anaylsis were executed.

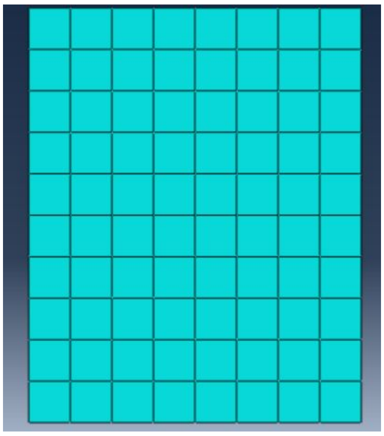

Figure 4.1. 2D planar model

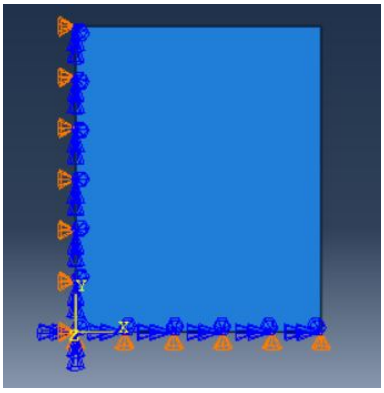

Figure 4.2. Defined boundary conditions

Figure 4.3 compares master relaxation moduli for Case 1 and Case 2 discussed in Section 3.6 and calculated with the Equation 2.16 against the ABAQUS analysis using Case 1 data.

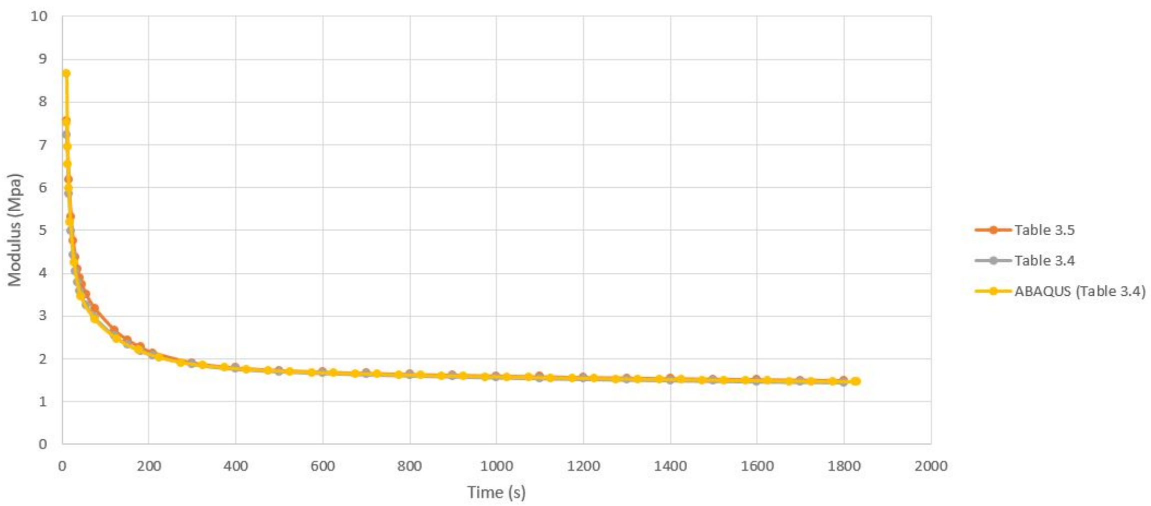

Figure 4.3. Time Domain Prony Series Verification via Abaqus

Figure 4.4 compares relaxation modulus at each temperature for validation of the Equation 3.7 and corresponding shift factors. Comparison is between the code output which is calculated from Equation 3.7 with the Prony series in Table 3.5 (case 2) and the ABAQUS analysis using the prony series in the study [12].

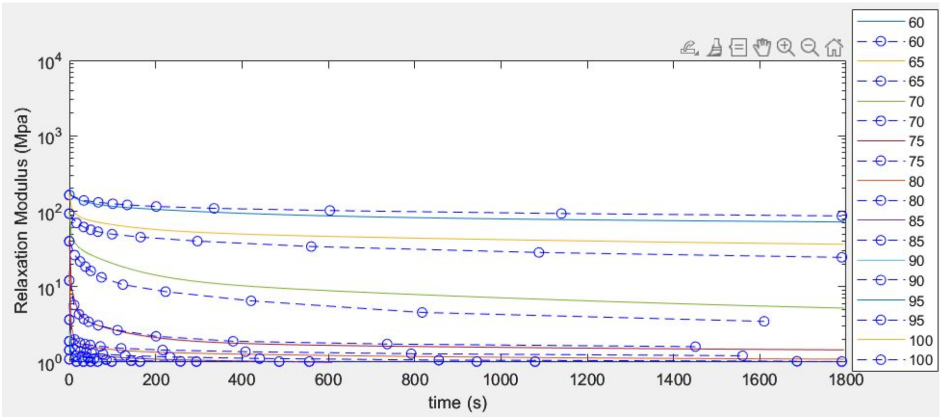

Figure 4.4. Relaxation modulus for each temperature calculated from Equation 3.8 using Table 3.5 against Abaqus analysis [12]

Figure 4.5 compares storage modulus for each temperature obtained from the study [12] against the results of the code. Parallel to Equation 3.8, frequency domain data for different temperatures is shifted according to the shift factors in terms of reduced frequency. As the code calculates shift factors and a Prony series, using,

$$E' = E_e + \sum_{1}^{N} \frac{E_i * \omega^2 * (\tau_i * (10^{(shift)+N-9)})^2}{1 + \omega^2 * (\tau_i * (10^{(shift+N-9)})^2}, \tag{4.1}$$

storage modulus for each temperature is calculated.

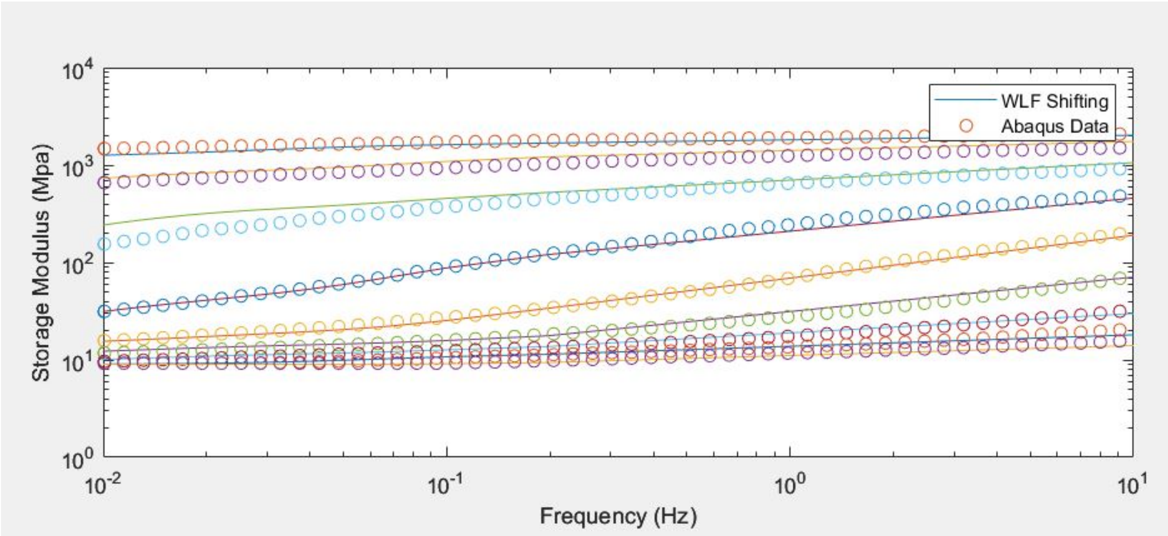

Figure 4.5. Verification of Storage modulus at each temperature

As a result of the methodology, using the calculated shift factors and Prony series, interconversion to time domain and to corresponig modulus at different temperatures is verified.

5. ANALYSIS EXAMPLE USING CALIBRATED MODEL

The validation of the code developed in Matlab and presented in Chapter 3 was done using ABAQUS. In particular , a circular brain specimen subjected to compression was analyzed [2]. Figure 5.1 illustrates the axisymmetric geometry which was used in the analysis. Figures 5.2 corresponds to 3D geometry obtained by sweeping the 2D model. CAX4R elements were used Material is defined as linear viscoelastic using the Prony series given in Table 3.4. Compression loading was applied as a displacement via a rigid plate. In time domain a dynamic analysis and in frequency domain a steady-state dynamic anaylsis were executed.

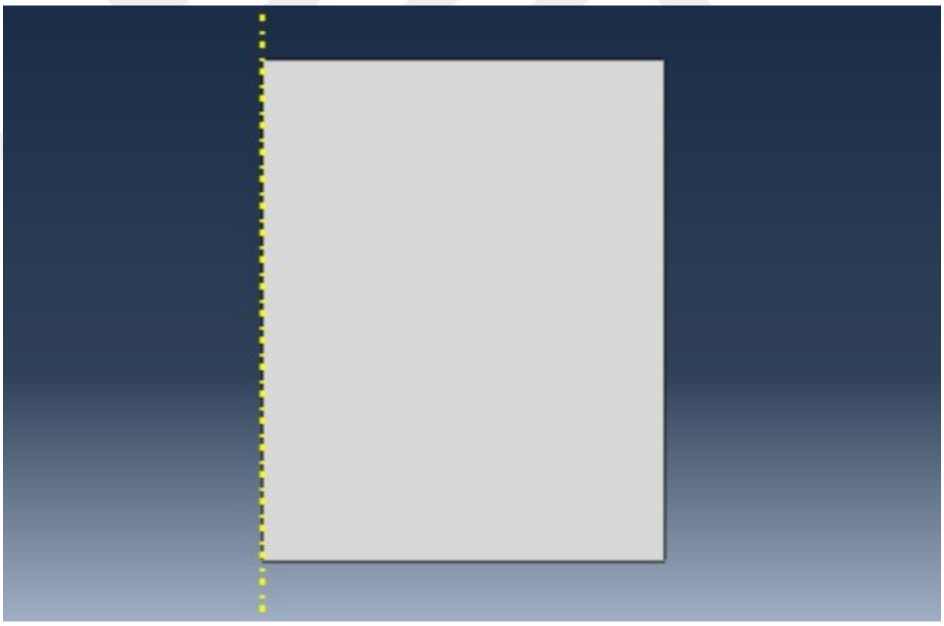

Figure 5.1. 2D axisymmetric model

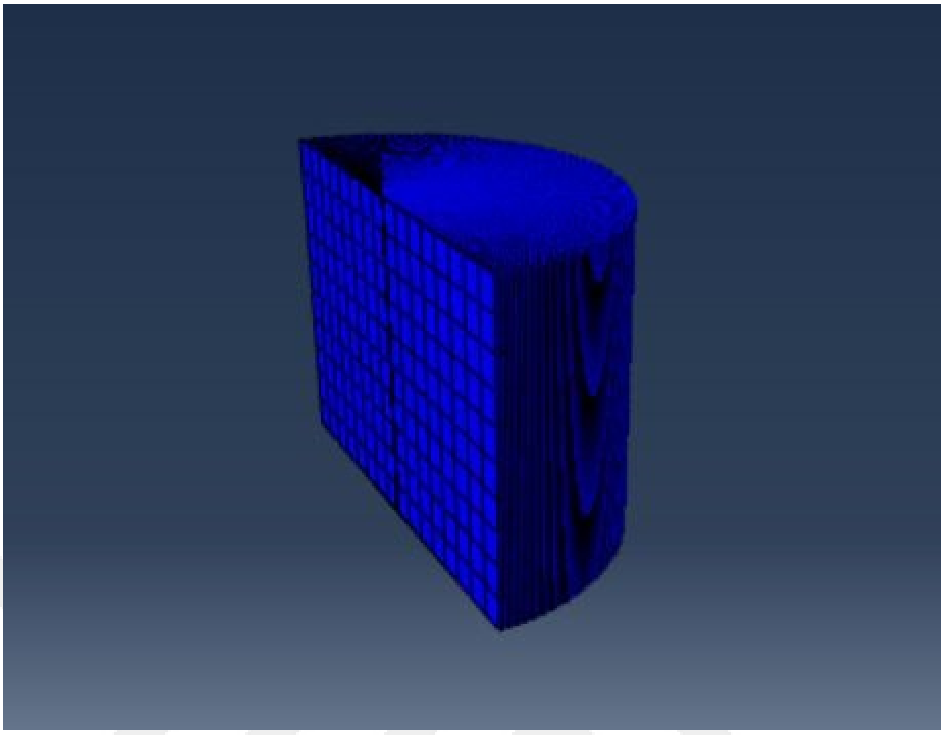

Figure 5.2. 3D sweeped model

Using the data given in [2] and the code developed in this study a Prony series was calculated and, than compared to the one given in [2]. Since the data extend from small to large frequencies, the fit for both the equilibrium (long-time) and instantaneous (short-time) moduli were accurate. To improve the Prony fit either equilibrium modulus or instantaneous modulus was prescribed, Fit 1 and Fit 2, respectively. Figures 5.3 and 5.4 compare the Prony series fits with that given in [Weiqi, 2021]. In this fit equilibrium modulus was prescribed. The Prony series values are given in Table 5.1.

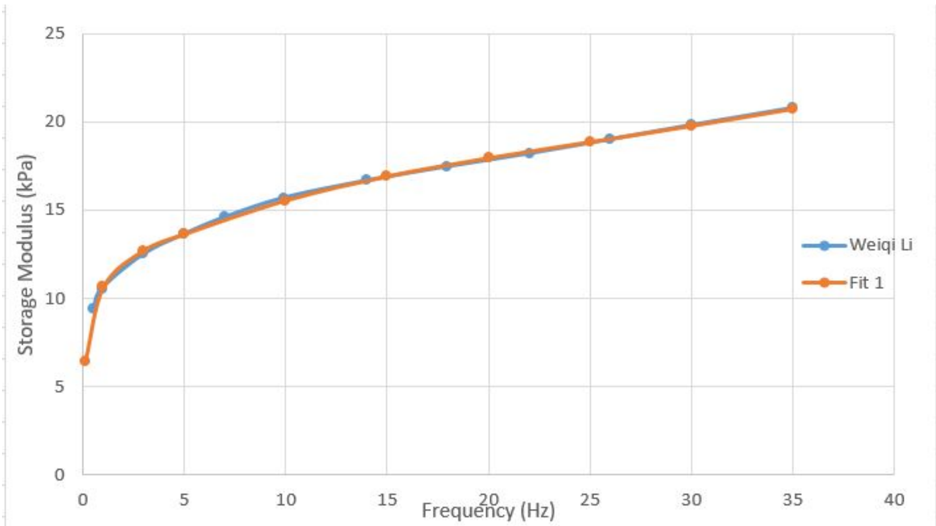

Figure 5.3. Storage modulus with equilibrium modulus constraint (Fit 1)

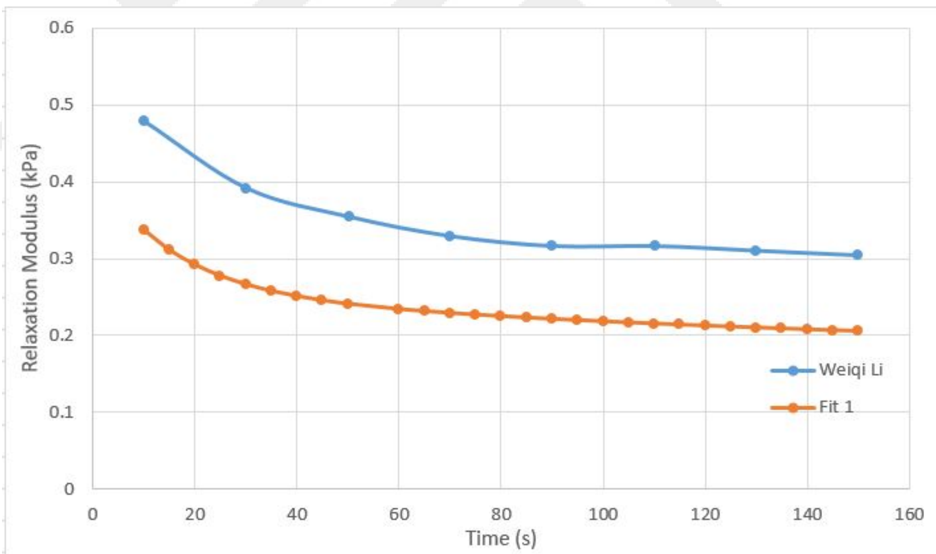

Figure 5.4. Relaxation modulus with equilibrium modulus constraint (Fit 1)

Table 5.1. Prony Series (Fit 1) With E_∞ Constraint.

	Cofficients, E_i (kPa)	**Relaxation times, τ (s)**
E_∞	0.48	
1	507.8381	1E-08
2	507.8381	1E-07
3	507.4952	0.000001
4	505.441	0.00001
5	660.0561	0.0001
6	2562.1	0.001
7	0.000561	0.01
8	5.3271	0.1
9	4.0336	1
10	4.468	10
11	1.6019	100
12	0.7248	1000
13	0.6173	10000
14	0.7374	100000

Figures 5.5 and 5.6 compare Prony series fits with that given in [2]. In this fit instanteneous modulus was prescribed. The Prony series values are given in Table 5.2.

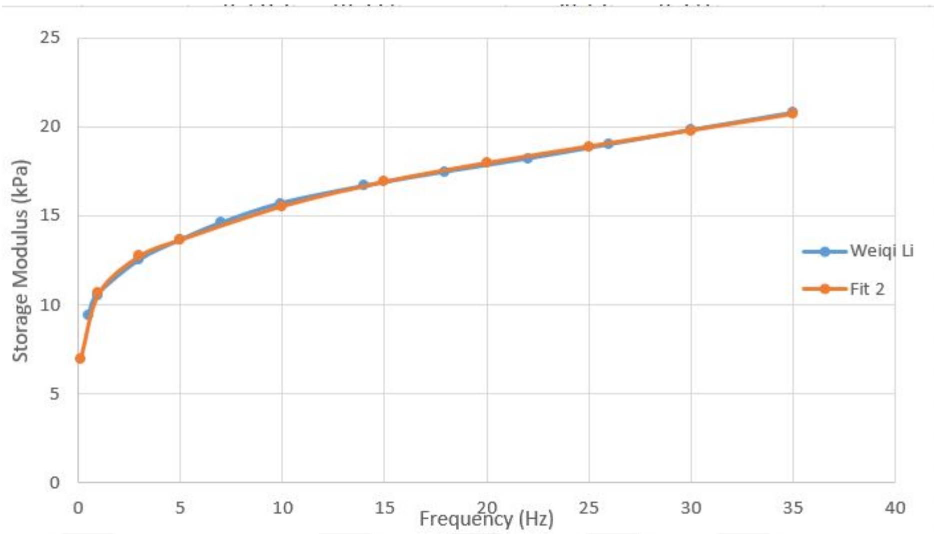

Figure 5.5. Storage modulus with instantaneous modulus Constraint (Fit 2)

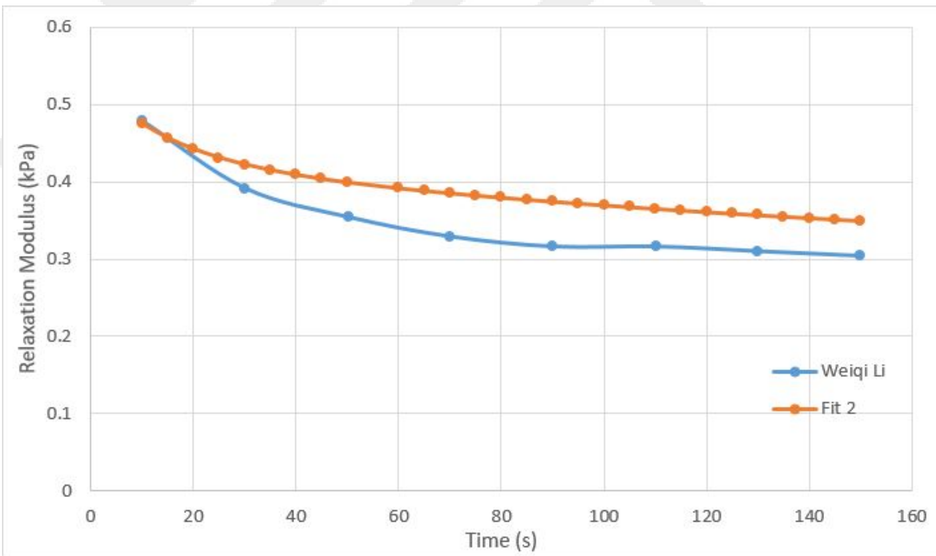

Figure 5.6. Relaxation modulus with instantaneous modulus constraint (Fit 2)

Table 5.2. Prony Series (Fit 2) With E_0 Constraint.

	Cofficients, E_i (kPa)	**Relaxation times, τ(s)**
E_∞	0.9256	
1	0.0378	1E-08
2	0.0378	1E-07
3	0.0378	0.000001
4	0.0323	0.00001
5	0.0362	0.0001
6	12.768	0.001
7	29.5194	0.01
8	5.1552	0.1
9	4.1237	1
10	3.298	10
11	0.9879	100
12	1.0793	1000
13	1.3371	10000
14	0.9438	100000

5.1. Cyclic Loading

Using the Prony fit with the instantaneous modulus constraint, Fit 2, a cyclic analysis was done in Abaqus. Same geometry and boundary conditions as described at the beginning of Chapter 5 were used. Sinusoidal strain was applied as seen in Figure 5.8 and the corresponding stress was calculated.

Figure 5.7 illustrates the resulting stress-strain graph and its comparison with [2].

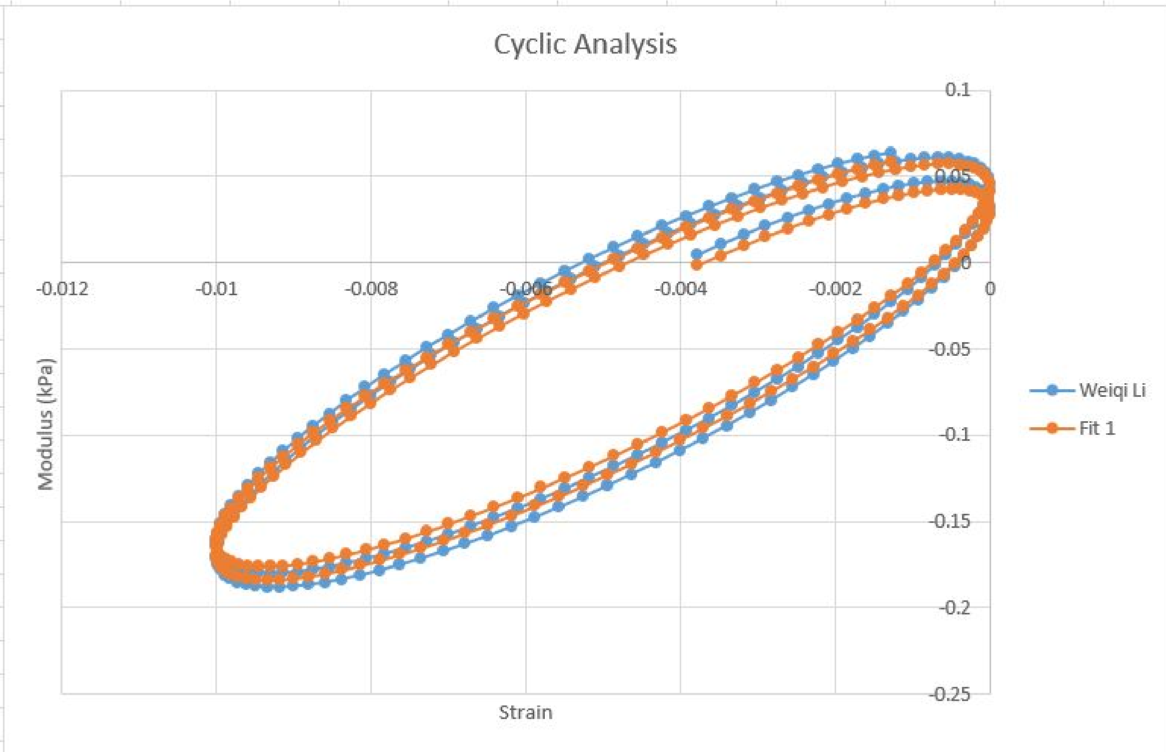

Figure 5.7. Cyclic loading.

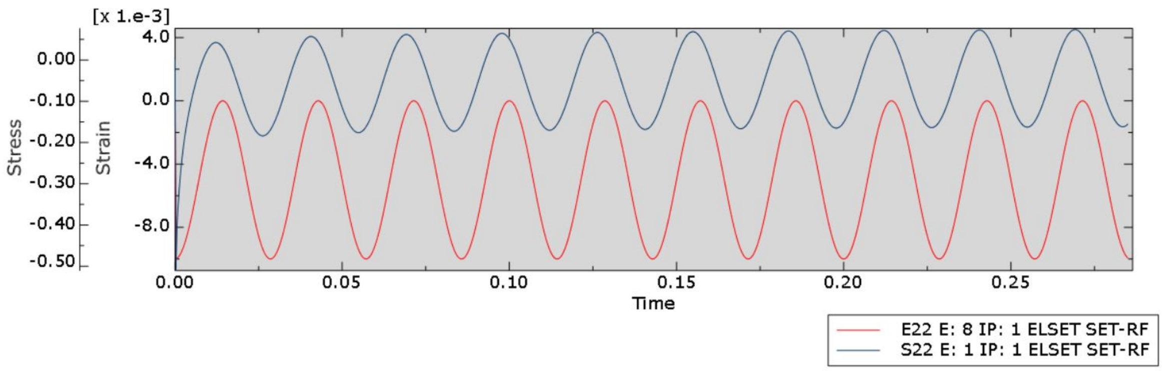

Figure 5.8. Sinusoidal applied displacement and the corresponding stress.

6. CONCLUSION

Throughout this study, a numerical methodology was employed to analyze different data sets, which included both frequency domain data and combined time and frequency domain data. Initially, the methodology focused on acquiring frequency domain data at various temperatures. This data was then utilized to construct a master curve that spans to a broader frequency range.

In Chapter 5, a different data set, as referenced in study [2], was analyzed. This data set included both frequency and time domain data. Given that the frequency domain data in this chapter has a narrower frequency range, a distinct approach was adopted. The code developed based on the master curve, which encompasses a wide range of frequencies, proved to be more advantageous.

The Prony series derived from the master curve (constructed from DMA data sets in different temperatures) is favored over those calculated from single DMA data sets (DMA data obtained in constant temperature). The master curve, with a frequency range from $10^{-}8$ Hz to 10^{8} Hz, enables a more accurate fitting of characteristic moduli, such as instantaneous and long-term modulus. In contrast, the single DMA data tested only spans from $10^{-}2$ Hz to 10^{2} Hz, which leads to suboptimal fits for the moduli.

Therefore, the main focus in Chapter 5 was to accurately capture the moduli by imposing constraints, as the data utilized included time domain information. Fitting the master curve is more reliable than fitting a narrow frequency range, even when adjustments are made according to constraints.

Future Work

Throughout this study, a methodology was developed. To further improve the fit for the Prony series and shift factor calculations, an additional method could be applied to the iterative shifting process. In this approach, an iterative vertical shift could be added after the horizontal shifting step, potentially enhancing the overall accuracy.

REFERENCES

1. Tapia-Romero, M. A., Dehonor-Gomez, M., Lugo-Uribe, L. E., "Prony Series Calculation for Viscoelastic Behavior Modeling of Structural Adhesives from DMA Data", *Engineering Research & Technology*, Vol. 21, No. 2, pp. 1-10, 2020.

2. Li, W., Shepherd, D. E. T., Espino, D. M., "Investigation of the Compressive Viscoelastic Properties of Brain Tissue Under Time and Frequency Dependent Loading Conditions", *Annals of Biomedical Engineering*, Vol. 49, No. 12, pp. 3737 - 3747, 2021.

3. Schwarzl, F. R., Struik, L. C. E., "Analysis of Relaxation Measurements", *Road Materials and Pavement Design*, Vol. 1, pp. 201-255, 1967.

4. Park, S. W., Schapery, R. A., "Methods of Interconversion Between Linear Viscoelastic Material Functions. Part I: A Numerical Method Based on Prony Series", *International Journal of Solids and Structures*, Vol. 36, No. 11, pp. 1653-1675, 1998.

5. Park, S. W., Schapery, R. A., "Methods of Interconversion Between Linear Viscoelastic Material Functions. Part II: An Approximate Analytical Method", *International Journal of Solids and Structures*, Vol. 36, No. 11, pp. 1677-1699, 1998.

6. Mun, S., Chehab, G. R., Kim, Y. R., "Determination of Time-Domain Viscoelastic Functions Using Optimized Interconversion Techniques", *Road Materials and Pavement Design*, Vol. 8, No. 2, pp. 351-365, 2007.

7. Tan, G., Wang, W., "Master Curve Establishment and Complex Modulus Evaluation of SBS-Modified Asphalt Mixture Reinforced with Basalt Fiber Based on Generalized Sigmoidal Model", *Polymers*, Vol. 12, No. 7, Article 1586, 2020.

8. Ferry, J. D., 1980, *Viscoelastic Properties of Polymers*, Springer, Boston.

9. Kattil, R., Sutton, M., Fuerte, R., Emri, I., "Time Temperature Superposition and Prony Series Coefficients of Asphalt Roof Shingle Material from Viscoelastic Creep Testing", in *Challenges in Mechanics of Time-Dependent Materials, Volume 2*, pp.105-114, Springer, Cham, 2018.

10. The MathWorks Inc., 2022, "MATLAB Version: 9.13.0 (R2022b)", Natick, Massachusetts: The MathWorks Inc., https://www.mathworks.com, accessed on December 2, 2024.

11. DSPE Knowledge Base, 2024, "Wire Flexure: Thermal Decoupling with Mixed Constraints Using Flexures and Rubber for Dynamics, Stiffness, and Damping", https://www.dspe.nl/knowledge/dppm-cases/wire-flexure-thermal-decoupling-with-mixed-constraints-using-flexures-and-rubber-for-dynamics-stiffness-and-damping, accessed on December 2, 2024.

12. Dalrymple, T., 2016, "Constructing a Hyper-Visco-TRS Model", *SUMULIA Community*, https://r1132100503382-eu1-3dswym.3dexperience.3ds.com/home?content-=swym:prd:R1132100503382:communitypost:ps40PvQYQAaqCQGzgHYklw, accessed on September 15, 2024.

13. Smith, M., 2009, *ABAQUS/Standard User's Manual, Version 6.9*, Dassault Systèmes Simulia Corp., https://www.3ds.com/products/simulia, accessed on October 10, 2024.